Minimal Catalytic Assemblies Can Oscillate Utilizing Feedback Loops

Antara Reja
IISER Kolkata
Sumit Pal
IISER Kolkata
Subhajit Bal
IISER Kolkata
Dibyendu Das (dasd@iiserkol.ac.in)
IISER Kolkata https://orcid.org/0000-0001-6597-8454

Article

Keywords:

Posted Date: May 10th, 2022

DOI: https://doi.org/10.21203/rs.3.rs-1235376/v1

Abstract

The light-dark cycles created from Earth's rotation helped in the emergence of extant cellular life that integrates evolved oscillatory networks to control circadian rhythms, cell division, metabolism and so forth. Out of equilibrium networks of organic chemical reactions with dynamic self-assembled structures that emerged from Darwin's nutrient-rich warm pond played crucial roles in spawning the protolife under a fluctuating environmental condition. Dynamic chemical networks with simple chemicals that can display emergent network dynamics can contribute to our understanding of complex behaviours from simple organic reactions. Here we have designed a single amino acid-based system that could self-assemble and oscillate under non-equilibrium conditions, importantly in the absence of evolved biocatalysts. The two-component based building block exploits pH driven non-covalent assembly and time-delayed accelerated catalysis from self-assembled state to install orthogonal feedback loops with a single batch of reactants. Modifications of these autonomous systems from purely synthetic molecules can enable the design of exceptional life-like materials and evolving systems with acute spatiotemporal control of properties.

Introduction

Chemical reaction networks capable of progressive phase transitions played vital roles in the chemical emergence of life and to drive the processes of extant biochemistry[1–9]. Living systems engage both non-covalent assembly and covalent linkages to achieve complex behaviours such as catalytic oscillatory reaction networks which are fueled by energy resources under the realm of non-equilibrium thermodynamics[10]. The periodic oscillation of these chemical transformations could have helped the systems to evolve with time towards the higher complexity seen in contemporary metabolic networks[11–13]. Inspired by such complex natural systems, attempts have been made to synthetically realize oscillating systems[14]. To install the capability to oscillate, the synthetic system should be integrated with the feedback loops as seen in the case of modern biochemical processes, from cell division to circadian rhythm and so on[15,16]. Thus far, oscillation has been demonstrated either by the use of 1) inorganic molecules in examples such as Belousov-Zhabotinsky (BZ) reactions, 2) exploiting evolved enzymes or DNA or 3) utilizing small organic molecules in absence of non-covalent interactions in an open system[17–21]. In contrast, no report has demonstrated a system that is capable to oscillate in a closed system utilizing non-covalent assembly and catalytic feedback loops generated from completely synthetic chemicals. The non-triviality arises in the installation of feedbacks in the absence of advanced biocatalysts in a closed system. Also, the dynamics of self-assembly of synthetic chemicals is generally limited by the relaxation towards chemical equilibrium[22]. Needless to say, if autonomous systems can be realized by utilizing purely synthetic molecules, then exceptional life-like materials can be accessed with acute spatiotemporal control of properties.

Here, we report a simple design featuring a single amino acid that can self-assemble and oscillate in a closed system. The building block exploits non-covalent assembly, accelerated catalysis from self-

assembled state and time delayed formation of a dynamic covalent bond, to introduce two feedback loops in a closed system with a single batch of reactants.

Results And Discussion

Towards our goal to access a minimal chemical-based system that can show oscillation, a self-assembly process was designed to install both negative and positive feedback loops with suitable time delays under non-equilibrium conditions. Firstly, if the assembly is catalytic and can promote its own degradation, then the negative feedback could be installed (Fig. 1a). Further, if one of the products of the catalytic degradation or waste can facilitate the regeneration of the assembly, the time delayed positive feedback loop will be installed (Fig. 1b). This coupling of negative and positive feedback loops might yield an oscillatory system (Fig. 1c). With these in mind, the building block **ABC** was rationally designed (Fig. 1d). The building block featured a kinetically stable but thermodynamically activated hydrophobic ester (**BC**, Fig. 1d). This aromatic ester had free aldehyde group that could couple via a dynamic imine bond with the amine group present in the polar residue (**A**) to access the amphiphilic building block **ABC** which may have the propensity to self-assemble (Fig. 1d). For the polar residue **A**, molecular histidine was used (Fig. 1d). Free histidine usually has poor hydrolytic roles yet they show an enhancement of their catalytic proficiencies when they are featured in supramolecular assemblies via multivalency, co-operative effects and so forth[3,23]. Finally, the dynamic imine bond was selected as this linkage is known for its acute responsiveness towards pH switches which was used to generate the second feedback (positive feedback). Hence, an ester was synthesized via the condensation of organic acid 4-formylbenzoic acid (**B**, Fig. 1d) and 4-nitrophenol (**C**), which was used as the hydrophobic part and upon catalytic hydrolysis would create a pH gradient to provide positive feedback towards the imine bond formation.

Temporal gelation at pH 7.5 buffer (one cycle)

We started with a simplified system where only one feedback (hydrolytic activity) would be operational while the other would be inoperative. Hence, the feedback that could generate from pH changes was deactivated by using a buffer system. **BC** was mixed with **A** at different molar concentrations with fixed molar ratio of 1:1 (DMSO/buffer solution, 60% v/v, pH 7.5). The samples with molar concentrations of 50 mM each (**A** and **BC**) gradually became viscous, followed by the transformation into self-supporting gel at around 2h (Fig. 2b). The gel showed weakening with time and manifested a gel-to-sol transition at 5h (Fig. 2b).

The transient gels were monitored by visible light scattering spectroscopy (λ = 700 nm) to measure the turbidity of the system. The rapid increase in turbidity was observed till 2.5h which exactly matched with the gelation time, followed by the gradual decrease that finally plateaued around ca. 11h (Fig. 2e). To gain more insight about the temporal gelation, transmission electron microscopy (TEM) was performed at different time intervals. TEM micrographs demonstrated the temporal generation of self-assembled fibrillar structures was responsible for gelation. At time ~0h, when the sample was in sol state, sparsely

populated fibrillar structures could be seen (Fig. 2c). However, at ca. 2h (gel state), the network like morphology was seen (Fig. 2c). After ca. 5h, when the sample turned to sol, very few fibrillar structures could be seen (Fig. 2c). Further, similar morphological transition was witnessed in scanning electron microscopy (SEM, Supplementary Fig. S1). Time-dependent rheology was performed to investigate the system in more detail on the macroscopic level. The gradual increase in storage modulus followed by the decrease (after 2h) in storage modulus, confirmed the temporal change in material property of the system (Supplementary Fig. S2 and S3).

At this point, to investigate the self-assembly and autonomous disassembly process, both the imine and ester bonds were monitored by different analytical techniques. To probe the formation of the imine bond, time dependent nuclear magnetic resonance (NMR) spectroscopy was performed. ^{1}H NMR of the sample containing **A** and **BC** (see Supplementary Information for more details) manifested the generation of imine with the proton peak at δ 8.41 ppm, which intensified till ca. 2h. The imine condensation even in a largely aqueous medium (~ 40% water) suggested the role of the self-assembly process, as observed in previous reports[24]. Notably, the intensity of the peak started to decline after 2-3h and suggested hydrolysis of the imine bond (Supplementary Fig. S4). The time gap in the increase and decrease of the imine peak intensity broadly corroborated with the lifetime of the gel. This suggested that the presence of the imine building block **ABC** is responsible for gelation and subsequent hydrolysis of the Schiff base leads to disassembly. Controls done without aldehyde group did not lead to gelation to suggest the importance of the imine building block (Supplementary Fig. S5). Further quantification of the extent of imine formation was not possible due to peak broadening that resulted from low mobility of the molecules at the gel state.

To probe the coupling of the transient gelation with the temporal formation of imine, the hydrolysis of the ester (**BC**) was monitored via time resolved HPLC. The rate of formation of **C** was monitored at λ= 318 nm (Fig. 2f). Notably, the rate profile showed an initial burst hydrolysis of the ester in the first 2.5h with catalytic rate 1.5 mM/h. This rise was followed by a gradual decline of the catalytic rates and rate plateaued after 5h. The initial burst suggested the gel state was catalytic while the sol state was unable to hydrolyse the remaining ester regardless of the presence of large amount of histidine. This suggested that the self-assembly process was coupled with the catalytic hydrolysis and subsequently was responsible for its own degradation, thus installing a negative feedback loop. It is important to note here that the product **B** also features the aldehyde functionality which can couple with the histidine via the imine bond. However, from NMR, no imine bond could be seen to be formed after 4h (Supplementary Fig. S4). Control experiments done with mixture of **C** with **A** and **B** did not show the generation of any imine proton peak from NMR. The mixture of **A** and **B** also did not access any gel or network like morphology. These results suggested that the self-assembling capability of the product (**AB** or **ABC**) is vital for the imine bond formation.

Temporal gelation at pH 6.5 buffer (one cycle)

As noted, the above experiments were done at pH 7.5. We were interested to investigate the system at a pH where the imine formation will be facilitated in the medium. For this, the pH of the medium was chosen to be 6.5 (DMSO/buffer, 0.1 M, 60% v/v) as low pH facilitates Schiff base formation via catalytic elimination of water[25]. At this pH, mixture of **A** and **BC** accessed a self-supporting gel within 0.5h, which was significantly faster than the gelation time required at pH 7.5 (Figs. 2d, e). The gel at pH 6.5 was stable for a longer time (lifetime of 4h compared to 2.5h in case of pH 7.5, Fig. 2g). Further, rapid rise in the turbidity in case of pH 6.5 compared to that observed for pH 7.5 supported the faster gelation in acidic pH (Fig. 2e). The prolonged lifetime was also confirmed from the turbidity measurement at pH 6.5. These observations suggested the rapid imine formation at acidic pH (6.5) facilitated greater extent of building block (**ABC**) generation that in turn led to longer lifetime of the self-assembled state. The greater extent of self-assembled networks was also supported by rheology measurements which showed improved mechanical strength of the gel (Fig. 2g, Supplementary Fig. S6 and S7).

The rate of hydrolysis at pH 6.5 was monitored by HPLC. The formation of **C** was seen to be accelerated significantly as it showed a burst release (for the first 0-3h, 4.4mM/h, Fig. 2e). Subsequently, the rate showed decline (for 3-5h, 1.7mM/h) before plateauing after 5h. The burst phase once again overlapped with the lifetime of the gel and reinforced the importance of the self-assembled catalytic microenvironment[22]. The rate of hydrolysis at pH 6.5 was almost three-fold higher than that was observed at pH 7.5 (Fig. 2f, inset). Higher hydrolytic rates at lower pH again supported the importance of the self-assemblies. The overall consumption of the ester was also significantly higher at the acidic pH.

Feedback from pH variation allows regelation (two cycles)

We noted that the remarkable differences in the lifetimes of gels, the extent of self-assembly and the subsequent negative feedback from hydrolysis was purely decided by the environmental pH (Figs.2e-g). We envisaged that if the system can itself register a gradual pH drop which is synchronized with the time delays in catalysis, it might be possible to realize an oscillatory gel; an unprecedented observation in literature thus far (Figs. 1c and 3a). The slowly forming waste (**B**) generated via the hydrolytic cleavage of **BC** can be the proton source to independently decrease the environmental pH that can consequently facilitate the regeneration of **ABC** utilizing the remaining esters in the medium to restart the cycle (Fig. 3a). Hence, unbuffered medium (Milli Q water) was used to achieve the pH switch within the medium. The mixture of **A** and **BC** (50: 50mM, **Sol1**) in 60% v/v DMSO/water showed an initial pH of 7.35 due to the presence of **A**. To monitor whether the proposed production of **B** was able to increase the acidity of the system, the pH was measured with time. Indeed, the pH of the system gradually declined from 7.35 to 6.1 in a span of ca. 48h (Fig. 3d). The visible light scattering measurement of the unbuffered system showed increase in turbidity till 2h that was followed by an expected decline. Remarkably, a distinct increase of turbidity was observed after 15h, which again peaked at 24h followed by the substantial decline in intensity (Fig. 3e). This observation suggested that the phenomenon of the creation of catalytic microenvironment was registered twice as a function of time with a single batch of reactant addition (closed system). Importantly, we could observe the sol-gel-sol-gel-sol transition (Fig. 3b). Starting from the initial sol state (**Sol1**), a self-supporting gel (**Gel1**) was accessed at around 1.5-2h which converted into

sol (**Sol2**) approximately within 5h (Fig. 3b). The regelation was observed at ca. 23-24h (**Gel2**, Fig. 3b). This was followed by the formation of viscous solution (**Sol3**,) in 60% of the samples while the rest 40% remained as weak gel after ca. 48h (done in 10 different sets of vials under identical experimental conditions, Fig. 3b).

Moreover, two cycles of assembly and disassembly were also suggested from time-dependent TEM investigations. Distinct network like morphologies was seen to be accessed at ca. 2h and 24h respectively, while in other time periods, significantly lesser extent of networks was observed (Fig. 3c). Time-resolved rheology could also register the temporal generation and regeneration of higher mechanical strength of the **Gel1** and **Gel2** in the 1st and 2nd cycle, respectively. The higher storage modulus (G') value of the **Gel1** (G' = 5567 Pa) and **Gel2** (G' = 4092 Pa) states compared to **Sol1** (G' = 709 Pa), **Sol2** (G' = 1572 Pa) and **Sol3** (G' = 295 Pa) underpinned the autonomous development of self-assembled structures at **Gel1** and **Gel2** states that resulted in gelation (Fig. 4a). To gain more details about the self-assembly process, time dependent fluorescence spectroscopy was performed. DPH was used as a dye, a well-known fluorescent reporter which shows augmented intensity when bound to hydrophobic microenvironment[26]. Expectedly, in the 1st cycle (**Sol1**-**Gel1**-**Sol2**), the gradual increase in fluorescence intensity was observed which peaked at **Gel1** state around 2h, then started to decrease at 3h (Fig. 4b). Around 24h re-intensification of fluorescence intensity was observed followed by decrease with ageing (Fig. 4b). The real time pH change in the macroscopic gel was monitored by using Methyl Red indicator that was added to the system from t~0h. The temporal change in colour of the medium from yellow to orange demonstrated the autonomous reduction of the pH within the system (Fig. 4c).

Further, time dependent NMR was performed with the unbuffered system. As expected, the generation of imine proton peak was observed at δ 8.41 ppm which gradually intensified at ca. 1h (**Gel1**) followed by the decline in peak intensity (Fig. 4d). The peak registered a resurgence in intensity at around 20-24h (**Gel2**, Fig. 4d). Subsequently, the imine proton peak started to diminish after 24h and plateaued around 48h. This result supported that indeed the waste **B** acted as positive feedback to regenerate the imine within the unbuffered system and consequently regelation was observed.

Extensive time-dependent HPLC was performed to monitor the release of **C** with respect to time and the hydrolytic activity was probed. As hypothesized, the positive feedback from pH which resulted in the re-formation of imine and subsequent regelation was expected to play a critical role in reviving the hydrolytic capability. Indeed, after the plateauing of rates (first cycle, 9-15h), an increase in the production rate of **C** could be detected again, at the similar timeline where regelation and re-intensification of imine were observed (Fig. 4e, orange band, 19-24h).

After confirming the temporal gelation (**Gel1**) followed by regelation (**Gel2**), the concentration distribution of the substrate as well as the products that were presented and produced within the medium were quantified from HPLC (Fig. 4e). Initially, at high pH the higher concentration of the **BC** drove the gelation thus overcoming the low imine conversion rate. Whereas in the case of **Gel2**, the low pH of the system helps in the rapid imine formation, thus the gel was formed even at low concentrations of **BC**. With further

decrease in pH no gel was formed because of insufficient gelation concentration at pH 6.1. Efforts are underway to increase the number of cycles of assembly and disassembly by varying the concentrations and molecular components.

Conclusions

Modern day organisms rely on elaborate and complex interconnected networks of non-equilibrium metabolic pathways with evolved enzymes for the construction (anabolism) and degradation (catabolism) of molecules for the maintenance of homeostasis[27,28]. Living systems engage both non-covalent assembly and covalent linkages to achieve such complex behaviours. This work demonstrates a simple chemical network that uses only two components, a single amino acid and a kinetically activated small molecular ester to demonstrate complex dynamic behavior such as the capability to show feedback-driven oscillation, with two cycles of assembly and disassembly with a single batch of reactants. For non-linearity, the system exploits non-covalent assembly which results in acceleration of catalysis, and time-delayed generation of pH gradient which leads to catalytic regeneration of a dynamic covalent bond, to install two feedbacks in the closed system. The minimal network suggests that complex behaviors that are usually associated with extant living systems, can indeed arise from a mixture of rudimentary chemicals even in the absence of any advanced biocatalytic systems.

Declarations

Data availability

The authors declare that all the data supporting the findings are available within this paper and the Supplementary Information files. Source data are provided with the manuscript.

Acknowledgment

D.D. is thankful to SB/SJF/2020-21/08 Grant for financial assistance. A.R. acknowledges IISER Kolkata and S.P. and S.B. acknowledge CSIR India for fellowships.

Author Contribution

D.D. conceived and supervised the overall project. A.R, S.P, and S.B conceived and performed all the experiments. All authors co-wrote the paper, discussed the results and commented on the manuscript.

Corresponding Author

dasd@iiserkol.ac.in

ORCID Dibyendu Das:0000-0001-6597-8454

References

1. Grzybowski, B. A. & Huck, W. T. The nanotechnology of life-inspired systems. *Nat. Nanotechnol.* **11**, 585–592 (2016).
2. Ragazzon, G. & Prins, L. J. Energy consumption in chemical fuel-driven self-assembly. *Nat. Nanotechnol.* **13**, 882–889 (2018).
3. Bal, S., Ghosh, C., Ghosh, T., Vijayaraghavan, R. K. & Das, D. Non-equilibrium polymerization of cross-β amyloid peptides for temporal control of electronic properties. *Angew. Chem. Int. Ed.* **59**, 13506–13510 (2020).
4. Ashkenasy, G., Hermans, T. M., Otto, S. & Taylor, A. F. Systems chemistry. *Chem. Soc. Rev.* **46**, 2543–2554 (2017).
5. Boekhoven, J. *et al.* Transient assembly of active materials fuelled by a chemical reaction. *Science* **349**, 1075–1079 (2015).
6. Debnath, S., Roy, S. & Ulijn, R. V. Peptide nanofibers with dynamic instability through nonequilibrium biocatalytic assembly. *J. Am. Chem. Soc.* **135**, 16789–92 (2013).
7. Ottelé, J., Hussain, A.S., Mayer, C. & Otto, S. Chance emergence of catalytic activity and promiscuity in a self-replicator. *Nat. Catal.* **3**, 547–553 (2020).
8. Miljanic, O. S. Small-molecule systems chemistry. *Chem* **2**, 502–524 (2017).
9. Astumian, R. D. Kinetic asymmetry allows macromolecular catalysts to drive an information ratchet. *Nat. Commun.* **10**, 3837 (2019).
10. Leira-Iglesias, J., Tassoni, A., Adachi, T., Stich, M. & Hermans, T. M. Oscillations, travelling fronts and patterns in a supramolecular system. *Nat. Nanotechnol.* **13**, 1021–1027 (2018).
11. Semenov, S. N. *et al.* Autocatalytic, bistable, oscillatory networks of biologically relevant organic reactions. *Nature* **537**, 656–660 (2016).
12. Ferrell, J. E., Tsai, T. Y. C. & Yang, Q. O. Modeling the cell cycle: why do certain circuits oscillate? *Cell* **144**, 874–885 (2011).
13. Hazen, R. M., Griffin, P. L., Carothers, J. M. & Szostak, J. W. Functional information and the emergence of biocomplexity. *Proc. Natl Acad. Sci. USA* **104**, 8574-8581 (2007).
14. Semenov, S. N. *et al.* Rational design of functional and tunable oscillating enzymatic networks. *Nat. Chem.* **7**, 160–165 (2015).
15. Pramanik, S. & Aprahamian, I. Hydrazone switch-based negative feedback loop. *J. Am. Chem. Soc.* **138**, 15142–15145 (2016).
16. Freeman, M. Feedback control of intercellular signalling in development. *Nature* **408**, 313–319 (2000).
17. Gyorgyi, L., Turányi, T. & Field, R. J. Mechanistic details of the oscillatory Belousov-Zhabotinskii reaction. *J. Phys. Chem.* **94**, 7162–7170 (1990).
18. Kim, J. & Winfree, E. Synthetic in vitro transcriptional oscillators. *Mol. Syst. Biol.* **7**, 465 (2011).
19. Novák, B. & Tyson, J. Design principles of biochemical oscillators. *Nat. Rev. Mol. Cell Biol.* **9**, 981–991 (2008).

20. Tsai, T. Y.-C. *et al.* Robust, tunable biological oscillations from interlinked positive and negative feedback loops. *Science* **321**, 126–129 (2008).
21. Orbán, M., Kurin-Csörgei, K. & Epstein, I. R. pH-Regulated chemical oscillators. *Acc. Chem. Res.* **48**, 593–601 (2015).
22. Omosun, T. O. *et al.* Catalytic diversity in self-propagating peptide assemblies. *Nat. Chem.* **9**, 805–809 (2017).
23. Chen, Y. *et al*. Self-Assembled peptide nano-superstructure towards enzyme mimicking hydrolysis. *Angew. Chem. Int. Ed.* **60**, 17164–17170 (2021).
24. Seoane, A., Brea, R. J., Fuertes, A., Podolsky, K. A. & Devaraj, N. K. Biomimetic generation and remodeling of phospholipid membranes by dynamic imine chemistry. *J. Am. Chem. Soc.* **140**, 8388–8391 (2018).
25. Clayden, J., Greeves, N., & Warren, S. G. *Organic chemistry* (Oxford University Press, 2012).
26. Poojari, C. *et al.* Behavior of the DPH fluorescence probe in membranes perturbed by drugs. *Chem. Phys. Lipids* **223**, 104784 (2019).
27. He, X. *et al.* Synthetic homeostatic materials with chemo-mechano-chemical self-regulation. *Nature* **487**, 214–218 (2012).
28. Spaet, T.H. Analytical review: hemostatic homeostasis. *Blood* **28**, 112–123 (1966).

Figures

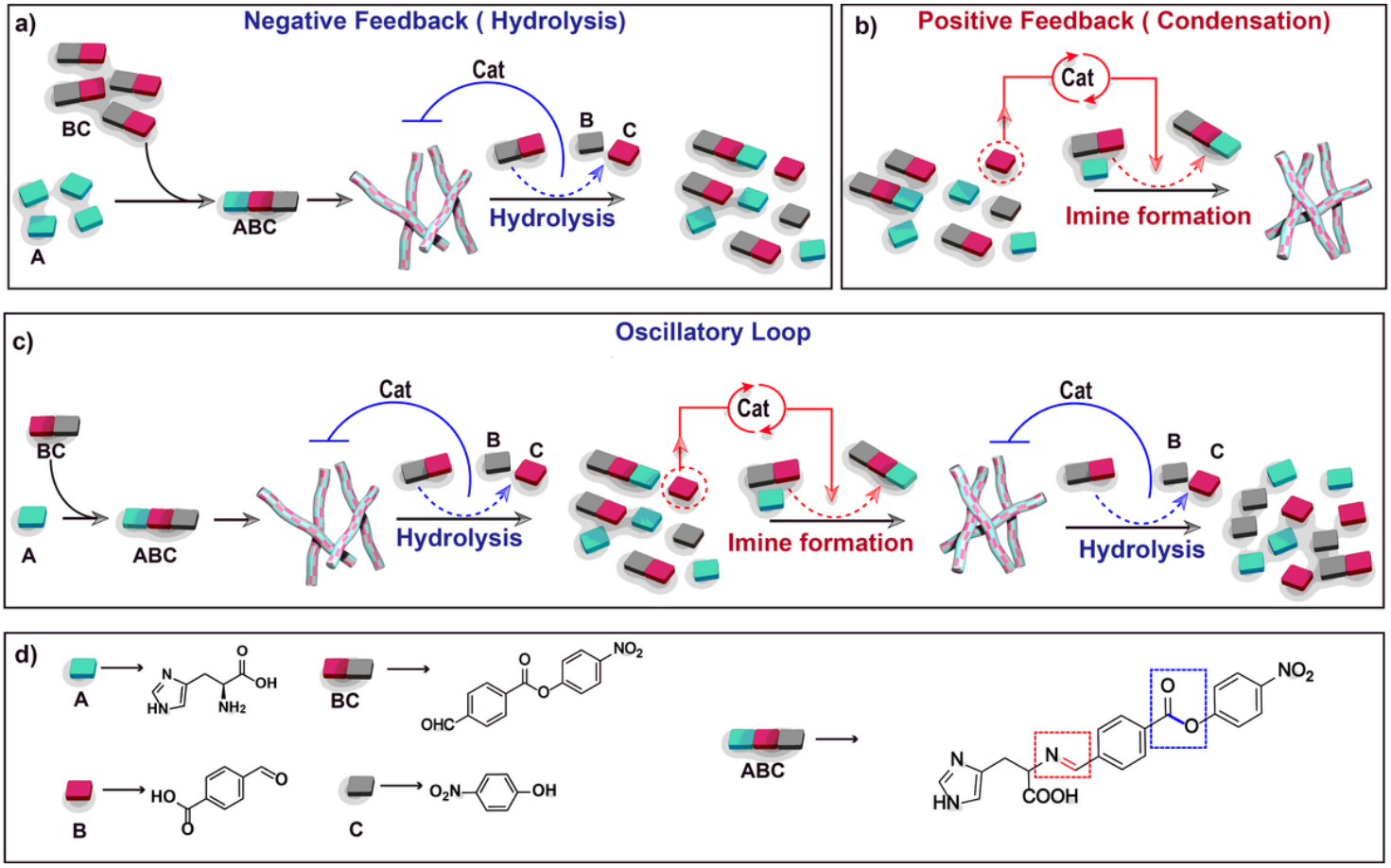

Figure 1

Schematic representation of dynamic self-assembly. Scheme showing **a)** the generation of assembly and subsequent disassembly due to catalysis (negative feedback), **b)** Catalytic regeneration of assembly from the product (positive feedback) of the disassembly. **c)** Integration of negative and positive feedback to make the oscillatory loop. **d)** Symbols and their corresponding chemical structures.

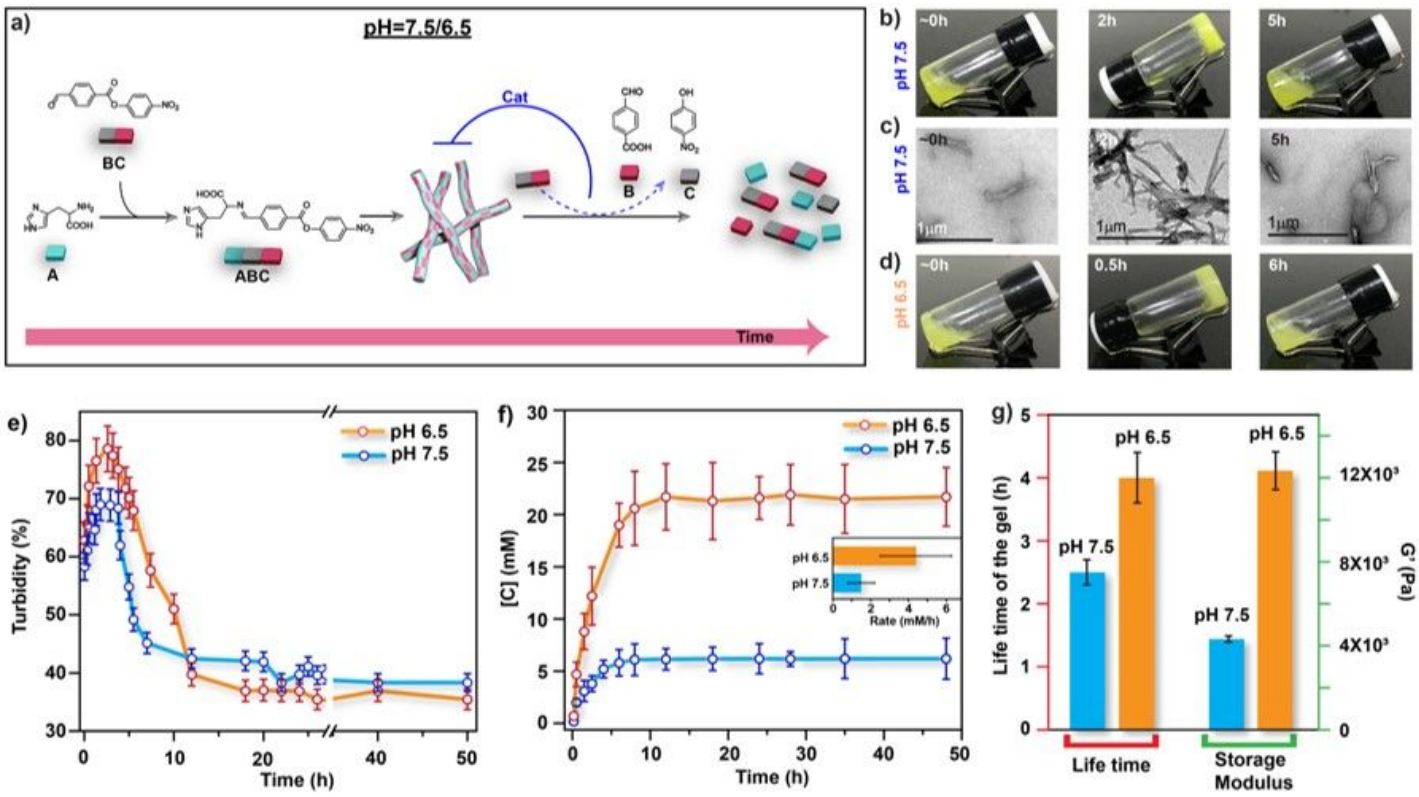

Figure 2

Gel formation and its catalytic activity at pH 7.5 & 6.5. a) Schematic representation of temporal generation of self-assembled structure at pH 7.5 and 6.5. Representative vial images at pH **b)** 7.5 and **d)** 6.5. **c)** Time dependent TEM images of pH 7.5 system. **e)** Temporal change in turbidity at pH 7.5 and 6.5. **f)** HPLC data of time dependent concentration change of generated **C** in pH 7.5 and 6.5 systems. Inset shows rate of **C** generation at pH 7.5 and 6.5 systems. **g)** Lifetime (red) and storage modulus (green) of the gel state at pH 7.5 and 6.5. Error bars represent standard deviations of triplicate experiments.

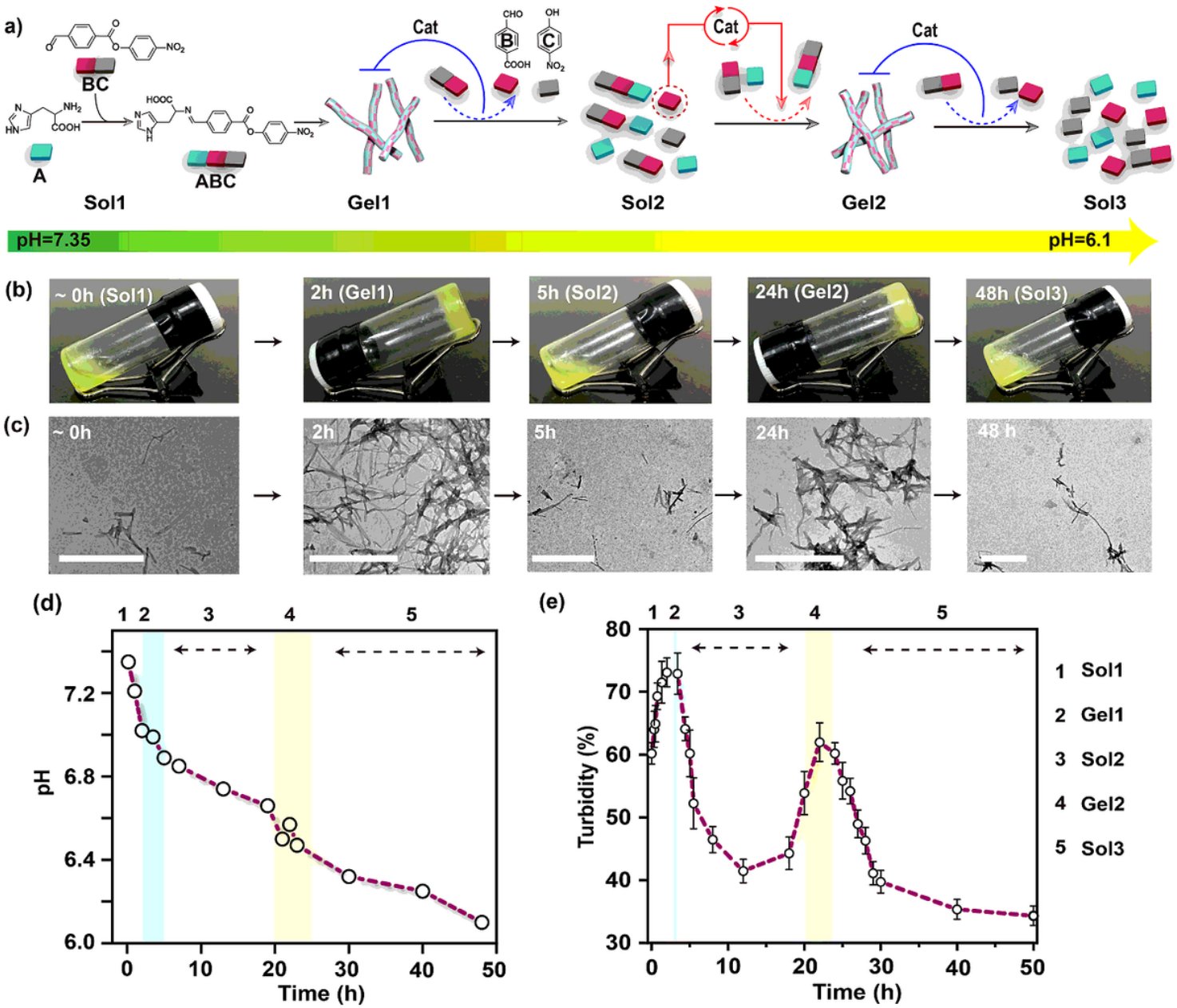

Figure 3

Switching of the pH allows the regeneration of assembly. a) Schematic representation of catalytic oscillation (two cycles) in unbuffered medium in a closed system. **b)** Representative vial images showing the temporal transition of different phases in unbuffered system (done in 10 different sets of vials under identical experimental conditions). After 48h, 6 out of 10 vials became viscous sol while the rest remained as weak gel. **c)** Time dependent TEM images. **d)** Temporal change of pH in unbuffered medium. **e)** Time dependent change of turbidity in unbuffered system using DPH (λ_{ex}= 350 nm). Error bars represent standard deviations of triplicate experiments.

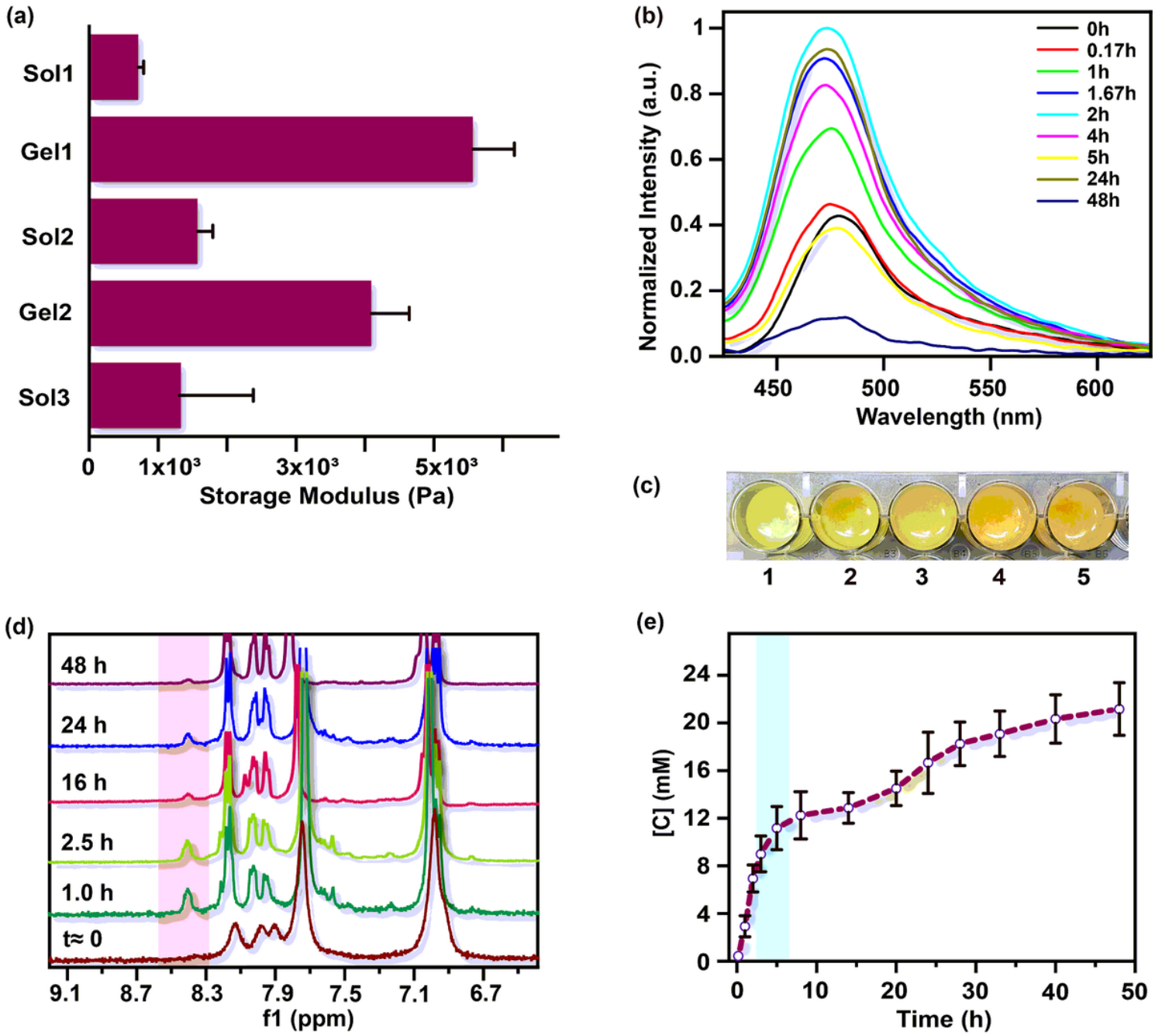

Figure 4

Temporal generation of self-assembly and its catalytic activity. a) Time dependent rheology showing the autonomous mechanical strength in the unbuffered system. **b)** Time dependent change in fluorescence intensity in the unbuffered system. **c)** pH dependent colour change of Methyl Red indicator in unbuffered system. **e)** Time dependent ^{1}H NMR in unbuffered medium. **e)** Time dependent HPLC showing the generation of **C** in unbuffered system. Error bars represent standard deviations of triplicate experiments.

Supplementary Files

This is a list of supplementary files associated with this preprint. Click to download.

- TOC.jpg
- SupplementaryInformation.docx
- Datafiles.zip